Ball milling as a way to produce magnetic and magnetocaloric materials

J. S. Blázquez[1], J. J. Ipus[1], L. M. Moreno-Ramírez[1], J. M. Álvarez-Gómez[1], D. Sánchez-Jiménez[1], S. Lozano-Pérez[2], V. Franco[1], A. Conde[1]

[1] Dpto. Física de la Materia Condensada, ICMSE-CSIC, Universidad de Sevilla, P.O. Box 1065, 41080 Sevilla, Spain.

[2] Department of Materials, University of Oxford, Oxford OX1 3PH, UK

Abstract

Ball milling (BM) is a well-established technique for producing different materials in powder shape. Dynamical analysis of BM helps to optimize the process through simple but general relations (e.g definition of an equivalent milling time). Concerning the area of study of magnetocaloric effect (MCE), BM is used in different ways: as a single step process (mechanical alloying), as an initial step to enhance mixing of the elements (e.g. to speed up the formation of the desired intermetallic phase) or as a final step (e.g. hydriding of La-Fe-Si). In this contribution, besides a simple description of the effects of some geometrical parameters on the power released during BM and a short review of the BM contribution to the research field of MCE, we will discuss the effect of the microstructure of the starting material and the granular shape inherent to BM on magnetic materials exhibiting MCE.

Keywords: ball milling and mechanical alloying; magnetocaloric effect

Corresponding author: J. S. Blázquez

e-mail: jsebas@us.es

1. Introduction

The versatility of ball milling (BM) techniques to produce metastable systems is well stablished [1-3]. The wide variety of materials that can be produced makes BM a transversal technique present in many different research fields. Therefore, it is worth noting the particular character of the samples produced (strongly disordered powder systems) when analyzing the results obtained from these samples. For example, in the case of magnetic properties [4], the existence of two different length scales is strongly relevant: the powder particle size (generally of the order of few microns) and the nanometric scale characterizing the crystalline structures (subnanometric scale in amorphous materials). These two scales combine to describe the soft magnetic behavior in mechanically alloyed powders [5, 6]: e.g. concerning the domain wall movement, the powder particle size implies an unavoidable limit to this mechanism, despite the averaging out of the magnetocrystalline anisotropy achieved in two-phase amorphous-nanocrystalline microstructures [7].

In the recent years, magnetocaloric effect (MCE), i. e. the adiabatic temperature change (or isothermal entropy change) of a sample when a magnetic field is applied or removed, has deserved the attention of the research community due to the possibilities of technological application in magnetic refrigeration at room temperature as a green technology [8, 9]. In order to get a high MCE response, the systems must have a strong variation of the magnetization with the temperature, found when a magnetic or magnetostructural transition occurs.

BM has been widely used to produce materials with significant MCE. Among the different factors affecting MCE response in BM powders, the multiphase character and the demagnetizing field effect, which affect the as-milled samples, were previously revised [10]. In this work, along these dependencies, we will point some other factors affecting MCE of samples for which BM was used as a production step.

This review starts with an introduction, followed by second section describing the dynamics of a planetary ball mill in the frame of a 2D single ball approach (neglecting sliding and rotation of the ball) [11, 12] where useful conclusions will be derived to compare different milling experiments. The literature on the use of BM for MCE materials is reviewed in the third section, which is divided depending on the use of BM as a single step, as a starting one to produce a precursor or as a final one to prepare the desired alloy in powder shape or by reactive milling. Once the utility of BM for MCE materials is reviewed, the importance of the homogenization of the precursor supersaturated solution will be presented and further discussed in the fourth section through two examples: boron incorporation to a transition metal matrix and La-Fe-Si system. The fifth section describes the effect of neglecting the shape of the powder on magnetic characterization, i.e. neglecting the demagnetizing field. The sixth section shortly

describes the effect of multiphase character on the MCE characterization and, finally, the main conclusions derived from this study are summarized.

2. Effect of some parameters on the power released to the powder in planetary mills

2.1 Ratio between disc and vial frequencies

Following the two dimensions geometry and single ball approximation used by Abdellaui and Gaffet [11] it is possible to calculate the normal force, *N*, exerted by the vial wall on the ball as:

$$N = m_b \left[\omega^2 \left(r_v - r_b \right) + \Omega^2 R \cos(\theta + \alpha) \right] \tag{1}$$

where ω and Ω are the angular frequencies of the vial and the disc, respectively, r_v, r_b and R are the radii of the vial, the ball and the main disc, respectively, m_b is the mass of the ball, θ and α are the angles rotated by the vial and the disc, respectively. It is worth mentioning that, from Eq. (1), the normal force becomes null at specific θ+α values depending on the ratios ω/Ω and r/R. Moreover, assuming that the ball stays in contact with the vial wall after the collision, the number of detachment and impact events per period of revolution is a constant only dependent on these ratios.

During the collision between the ball and the wall, some powder should be trapped absorbing part of the energy released. Assuming that the ball stays stuck to the wall after the collision, this energy can be calculated as [12]:

$$\Delta E_C = m_b \Omega^2 R r \frac{\omega}{\Omega} \left[\cos\left\{ \left(\Omega + \omega \right) t_d \right\} - \cos\left\{ \left(\Omega + \omega \right) \left(t_d + t_f \right) + \delta \right\} \right] \tag{2}$$

where $r=r_v-r_b$, t_d and t_f are the detachment time and the flying time of the ball and δ is the angle between the detachment point and the impact point of the vial. ΔE_C~7 J/kg per collision for ω/Ω=-2, Ω=200 rpm, R=24.6 cm and r_v-r_b=3.25 cm (values typical for the Fritsch Pulverisette P4 Vario mill used in all the experiments along this study). Other authors have estimated similar values of ΔE_C using different approximations [13]. The power released can be calculated dividing the released energy by the time between collisions as:

$$P_T = \frac{\Delta E_C}{t_d + t_f} = k \Omega^3 \tag{3}$$

As the number of collisions during a period is a constant of the system, as shortly described above and in more detail in [12], the power released during milling is proportional to the third power of the frequency as indicated in Eq. (3). This allowed us to define an equivalent milling time to compare milling experiments at different Ω values [12]. k is a constant depending on the milling parameters. It is worth mentioning that other mechanisms of energy

transfer, such as friction, do not alter the linear dependency with Ω^3 [12]. Other authors [14] use the dose, D_m, defined as the energy transferred to the powder during the milling process per unit mass of processed powder to describe the milling process:

$$D_m = \frac{P_T t}{m_p} \propto \Omega^3 t \tag{4}$$

The dose is generally found to describe the intensity of the milling process [1].

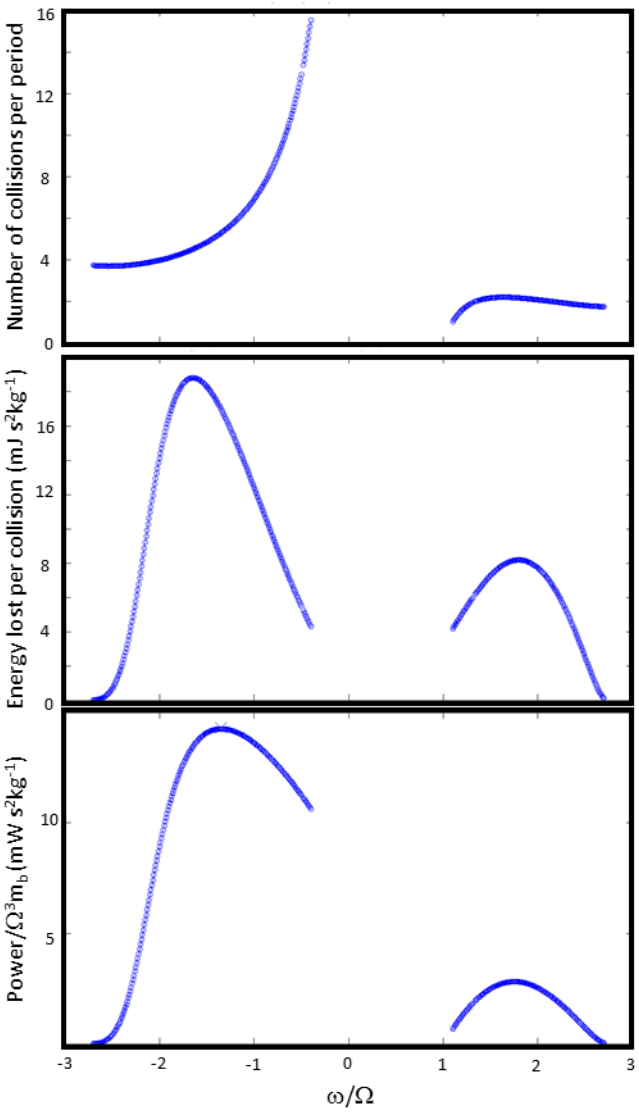

Figure 1: Number of collisions per period (upper panel); energy released per collision and ball mass (middle panel); and power released per unit mass of ball divided by Ω^3 as a function of ω/Ω.

We solved numerically the equations describing the 2D movement of a single ball in a planetary mill and (using the geometrical parameters typical for P4 mill with $(R/r)^{0.5}$=2.75) we

obtain the dependence of P_T/Ω^3 and we plot the results in figure 1. Despite the simplicity of the model, some interesting conclusions can be derived:

There are two maxima in the plot, one corresponding to positive values of ω/Ω and the other one to negative ones. The maximum observed at negative values of ω/Ω should be the optimum operation condition to minimize the milling time (assuming that the transformation should depend only on the dose or the energy accumulated by the powder).

As it can be deduced from Eq. (1), the ball should remain attached to the wall if $\omega/\Omega>(R/r)^{0.5}$. This leads, in the present case, to a range of frequency ratios between -2.75 and 2.75. As ω/Ω increases from -2.75, both the energy per collision and the number of collisions increase. However, although the number of collisions continuously increases as ω/Ω approaches zero, after a certain value of ω/Ω (see figure 1) these collisions become less energetic and thus the power decreases. For positive values of $\omega/\Omega>1$, the number of collisions per period is almost constant but lower than the values obtained for $\omega/\Omega<0$. Moreover the energy per collision is also generally lower.

We tried to compare the predictions of this simple model with experimental measurements of the temperature increase inside the vial. On the one hand, this temperature must increase due to the mechanical heating, Q_M, proportional to Ω^3 and, on the other hand, heat must be lost through conduction to the environment, Q_L. Therefore, a simple law relates the temperature difference, ΔT, inside the vial with respect to the environment and the frequency, Ω:

$$C\frac{dT}{dt}=\frac{d\left(Q_M+Q_L\right)}{dt}=A\Omega^3-B\Delta T \tag{5}$$

where C is the heat capacity of the system, T is the temperature, t the time, and A and B, constants. In stationary conditions, Eq. (5) is simplified to:

$$\Delta T=\frac{A}{B}\Omega^3 \tag{6}$$

And thus, ΔT must be proportional to the power released and thus the temperature achieved at a certain value of Ω (350 rpm in our case) will help us to analyze the dependence on the geometry and ω/Ω ratio. Therefore, in figure 2 we show ΔT achieved after 1 h milling at 350 rpm for different values of ω/Ω with $(R/r)^{0.5}$=2.75 and 50 balls of 10 mm diameter (inset shows the predicted linearity of ΔT with Ω^3). The P4 mill limits the maximum Ω to be used depending on the ω/Ω ratio and thus the study has been limited to a range for which 350 rpm can be used. Qualitatively, the curve is similar to that shown in Fig. 1. However, the maximum is shifted to

higher values of ω/Ω. This is a consequence of the strong approximations of the model used, particularly due to the single ball approximation. In order to obtain a significant signal, many balls are needed and, even neglecting the interaction between them, the effective radius of the vial would not be the same for each ball. Figure 3 shows the effect of reducing the effective radius of the vial in the ω/Ω<0 branch of figure 1. As observed in the experimental data, the maximum is shifted to higher absolute values of ω/Ω.

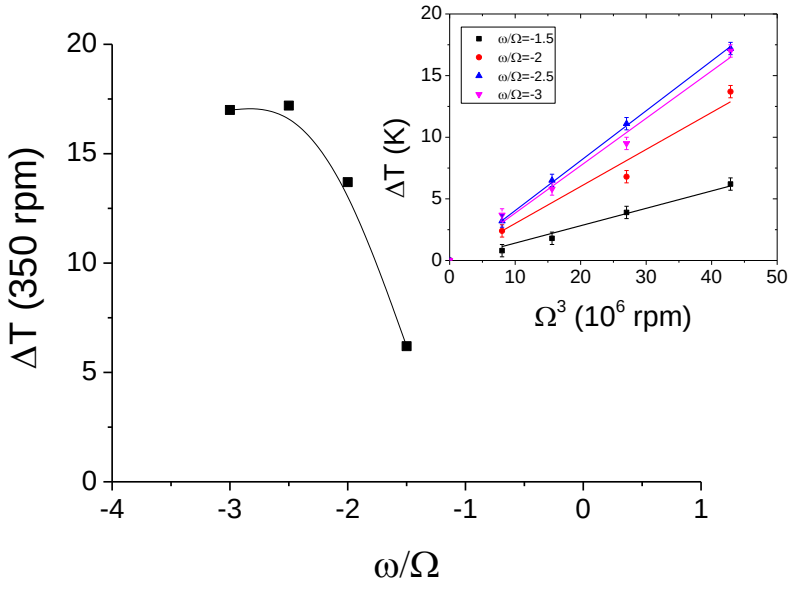

Figure 2. ΔT after 1 h milling at 350 rpm for 50 steel balls of 10 mm diameter as a function of the ω/Ω ratio. Inset: linear dependence of ΔT with Ω³.

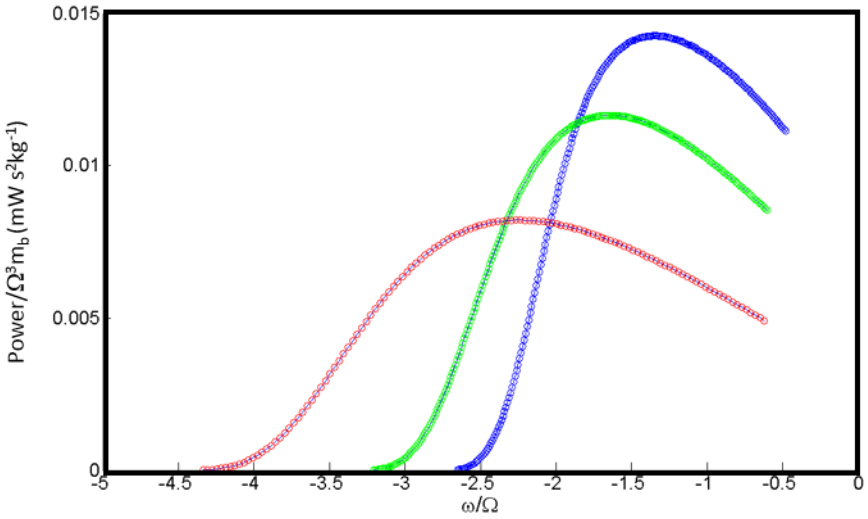

Figure 3. P_T/Ω^3 vs. ω/Ω for different values of $r=r_v-n\cdot r_b$ (r_v=37.5 and r_b=5 mm, the radii of the vial and the ball, respectively) with n=1 (blue), 3 (green) and 5 (red).

2.2 Diameter of the balls: an indirect change of the geometry

As shown previously, the experimental results deviate from the single ball predictions. However, the simplicity of this approximation and the simple relations obtained are very attractive for an easy comparison between milling processes performed in different labs. Concerning the dependence of milling dose on the ball parameters, it has been generally assumed a roughly linear dependence with the number of balls or indirectly the powder to balls mass ratio was considered to indicate how energetic the milling performed was [1]. In this section, we will experimentally describe that this relation is not that simple but there is a clear dependence of the power released on the radius of the balls (steel balls were used) when keeping constant the mass of the balls.

Figure 4 shows the dependence of ΔT at 350 rpm (and thus of P_T) after 30 min milling on the ball radius (2.5, 5, 10 and 20 mm), keeping the total ball mass constant (number of balls: 512, 64, 8 and 1, respectively) for different values of ω/Ω. There is a close to linear relationship, decreasing ΔT as the radius increases. This relationship could be understood from Eq. (2) which gave us an approximate expression for the energy of collision. If we explicitly show the dependence of this parameter per unit mass of ball on the radius of the ball, Eq. (2) will result:

$$\frac{\Delta E_C}{m_b} = \Omega^2 R\left(r_v - r_b\right)\frac{\omega}{\Omega} f\left\{\left(\Omega+\omega\right), t_d, t_f, \delta\right\} \qquad (7)$$

Linear fittings to the data for the optimum milling conditions (ω/Ω=-2.5 and -3) result on slope values of -0.38±0.04 and -0.44±0.03 K/mm for ω/Ω=-2.5 and -3, respectively, and intercept values of 15.8±1.0 and 19.5±0.7 K. If we compare the two lines obtained for each ω/Ω, following Eq. (7), both ratios (between the slopes and the intercept) should be equal to the ratio between ω/Ω values, which is 2.5/3~0.83. In the case of the slopes, the ratio is 0.86±0.15, and in the case of the intercepts, the ratio is 0.81±0.08, in good agreement with Eq. (7). For the other two ratios studied, the linearity is worse and the results deviate from the predictions of Eq. (7) (see inset of Fig. 4). Moreover, from Eq. (7), the diameter of the vial might result after dividing each intercept by the corresponding slope, being 46±15, 41±7, 44±5 and 44±12 mm for ω/Ω=-2, -2.5, -3 and -3.5, respectively. Although the obtained value is independent of ω/Ω, it is smaller than the actual one ($2r_{vial}$=75 mm), in agreement with the shift observed in Fig. 2 for the experimentally found maximum of the power released to more negative ω/Ω ratios than the predicted one from the single ball model. In fact, as the number of balls increases, the effective radius of the vial (the radius of the available trajectory of a ball inside the vial) should decrease.

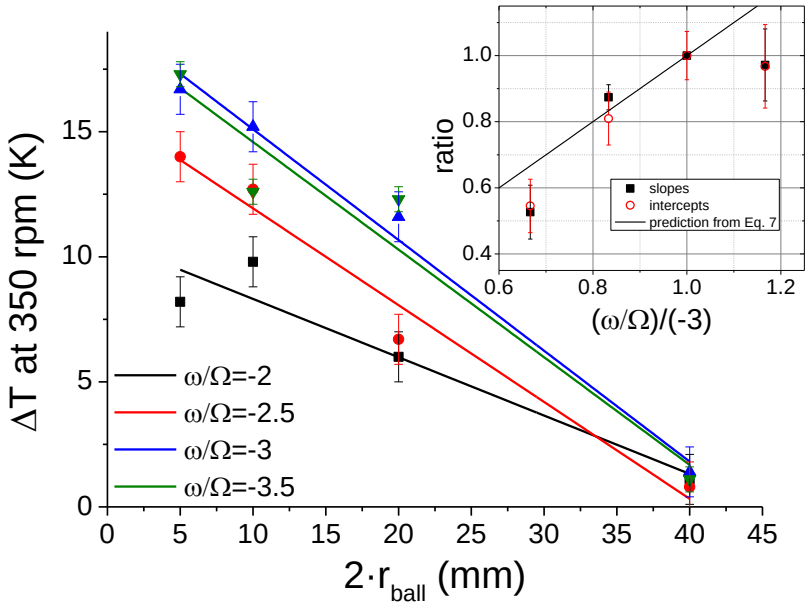

Figure 4. ΔT at Ω=350 rpm vs. the diameter of the balls. The total mass of balls used is constant.

3. Ball milling to produce MCE materials in the literature

Concerning the use of ball milling techniques to produce materials with significant MCE, several ways can be found in the literature that can be roughly divided in: one step production, BM as a first step, and BM as a final step in the production of the samples.

3.1 Single step production

The ability of BM to produce alloys and complexes via mechanical alloying or mechanochemical reactions makes this technique attractive to produce many different systems, such as Gd-based amorphous alloys [15-17], Fe-based amorphous alloys [18-20], Co-based amorphous alloys [21], FeNi metastable phases [22-25], Heusler alloys [26], oxides [27-29], maganites [30, 31] and, recently, Gd-based borohydrides prepared by a mechanochemistry route [32].

Due to the high concentration of defects, BM (or mechanical alloying) can be frequently followed by some annealing process or by sintering to obtain bulk samples from the powders. However, hot compaction is not trivial when the as-milled microstructure is needed to be preserved, as for amorphous alloys [33]. Sintering is typically used for perovskite-type systems [34, 35]. In this case, wet milling enhances the aspect ratio of the powder and the MCE response with respect to dry milling [36]. Wet milling also leads to better MCE response for spinel Zn-ferrites [37].

Some studies compare BM samples to those produced using rapid quenching techniques (e. g. MnFe(PGe) samples [38], Heusler [39] or transition metal based amorphous alloys [21]). Besides the general broadening of the transition due to induced microstrains and disorder, differences in the transition temperature can be found, ascribed to a non-perfect dilution of the elements (e.g. boron as will be shown below) and thus to a departure from the nominal composition.

3.2 BM as a first step

When volatile elements such P, As or Mn are present in the target alloys, BM can be used to avoid excessive losses, preparing a precursor alloy which should require annealing to develop the desired phase. Examples can be found in $Mn_5(GeSb)_3$ [40], $Fe_2(PAs)$ [41, 42], MnFe(PGe) [43], MnFe(PAsGe) [44-48], $Fe_2Mn(SiGe)$ [49, 50], MnFe(PSiB) [51], (MnCr)As [52-54] or $(CoMn)_2(PSi)$ [55, 56].

The homogeneous dispersion of elements that can be easily obtained by milling even for elements with positive enthalpy of mixing, ΔH^{mix} [57], makes BM an useful technique for FeMn-based alloys (ΔH^{mix}=0 kJ/mol for Mn-Fe), (MnCr)As [52] (ΔH^{mix}=+2 kJ/mol for Mn-Cr) or $La(FeSi)_{13}$ family [58] (ΔH^{mix}=+5 kJ/mol for La-Fe). Moreover, the good mixing at short length scales obtained by BM is responsible for the decrease of the annealing time to form a desired intermetallic with respect to that of ingots prepared by arc melting (e.g. MnAs-type [52, 59]; $La(FeSi)_{13}$ [60, 61] or $(PrDy)_2Fe_{17}$ [62].

BM can be used also to produce graded materials to build up functional tapes for MCE applications [63] or controlling the powder size to embed it in a polymer as did for (LaPrCe)$(FeMnCoSi)_{13}$-H [64]. Studies on spark plasma sintering (SPS) of mechanically alloyed systems followed by annealing are also found in the literature [65]: However, the latter step is not always needed: as for cementite [66] or as it was shown by Patissier et al. [67], who obtained ~90 % of $NaZn_{13}$-type phase after SPS, unlike weeks of annealing by conventional processes. Bartok et al. [68] have recently compared the MCE response of BM powder and sintered by spark plasma (1223 K, 30 min) and conventional technique (1123 K, 20 h) for $Mn_{1.3}Fe_{0.65}P_{0.5}Si_{0.5}$ system. Powders exhibited a smoother transition and the authors found significant differences only in the first cooling between both sintered samples.

2.4 BM as a final step

BM can be straightforwardly used to pulverize a material to observe the MCE in micrometer powder samples (e.g. $Tb_5(SiGe)_4$ [69], Gd [70], $Gd_5Si_2Ge_2$ [71], $Gd(NiFe)_3$ [72]. In the case of $RE_5(SiGe)_4$ (RE=Gd or Tb), pulverization leads to a weakening of the MCE signal for Gd but an enhancement for Tb, ascribed to the enhancement of magnetostructural coupling

driven by strains [73]. In the case of Fe-based amorphous alloys [74], the expansion of the interatomic distance enhances magnetism of the system.

In crystalline systems, the strong mechanical stresses applied during ball milling generally lead to a reduction of the crystal size down to nanometric scales [3], allowing both the stabilization of out stoichiometric concentrations in nanocrystals and the presence of a large fraction of boundary regions to accumulate defects. Before the rise of MCE studies at room temperature, BM was already used in this sense by Shao et al. [75] to study nanometric samples of Gd binary alloys. More recently, Llamazares et al. [76] studied the effect of BM on Pr_2Fe_{17} and Alvarez et al. on Nd_2Fe_{17} [77]. Zhang et al. [78] used BM to tune the particle and crystal size of CrO_2. Other examples are Laves phases [79], Gd-garnets [80], Heusler alloys [81, 82], $Gd_5Si_2Ge_2$ [83], pseudo-Laves phases [84], Nd_5Ge_3 [85], manganites [86, 87], clathrates [88], and $NdMn_2Ge_2$ [89].

It is generally observed that the MCE response becomes broader but weaker. As an example, this trend is found for NiMnGa, for which milling as-cast samples reduces their MCE signal but the response is recovered after annealing [90]. In the aim to optimize the magnetocaloric performance of a material, a broad and flat peak should be positive when magnetic entropy change values are not strongly reduced. In this sense, composite materials have been proposed [91] and BM should easily supply out stoichiometric or slightly out of equilibrium systems enabling to tune the transition temperature [72, 92, 93]. A compromise to obtain a high refrigerant capacity without significant values of magnetic entropy change can be found.

One of the most promising material for MCE at room temperature is the $La(FeSi)_{13}$ family [94]. Hydriding of this family shifts transition to room temperature without reducing MCE response (unlike Co addition). Reactive milling in hydrogen has been shown to supply similar results to samples annealed in hydrogen atmosphere [95]. The alternative offered is very attractive as dangerous processes can be avoided [96]. Moreover, a decrease of the thermal hysteresis in samples produced by this reactive milling has been found [97]. This reduction of thermal hysteresis was also found in mechanically alloyed Mn(AsP) [98].

4. Effect of the microstructure of the starting material

4.1 Boron integration in a transition metal matrix

In the case of magnetic alloys, boron is an element found in both extreme systems, the softest (FINEMET [99]) and among the hardest (NdFeB [100]) materials. However, the incorporation of boron via mechanical alloying to Fe or Co matrices is not trivial, due to the low solubility of this element in bcc Fe and hcp or fcc Co [57]. Boron is a brittle and hard material and boron inclusions remain without mixing in the matrix even after mechanical amorphization

of the material [101, 102]. However, the low atomic number Z of this element prevents the identification of B-rich phases by X-ray diffraction (XRD) or localized enriched regions by conventional X-ray analytical techniques. As an example, figure 5 shows the square of the atomic scattering factor, $|f_{at}|^2$, as fitted by Doyle and Turner [103] for B (Z=5) and Fe (Z=26). The latter element, the most abundant in magnetic materials, exhibits around two orders of magnitude bigger values of $|f_{at}|^2$ than B, which prevents the detection of remaining rich-B phases in magnetic alloys by XRD.

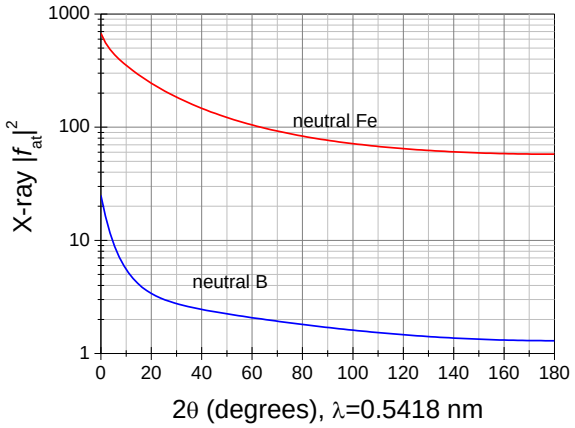

Figure 5. Square of X-ray scattering factor for Fe and B versus 2θ angle and Cu-Kα wavelength.

Previous studies have shown that the starting microstructure of boron can influence the degree of incorporation of this element via mechanical alloying. Those studies concluded that incorporation of boron to an amorphous Fe(Nb) matrix enhances when using amorphous boron instead of crystalline one but incorporation is almost complete when starting boron is forming an intermetallic, such as FeB phase [104]. Figure 6 shows the degree of incorporation of boron into the amorphous matrix as a function of the starting microstructure used. The values were obtained after comparing the Curie temperature, T_C, of the amorphous phase obtained by mechanical alloying with that of a melt-spun amorphous alloy [104]. It was assumed a decrease of ~25 K per at. % of B as it occurs for Fe-B amorphous binary alloys [105].

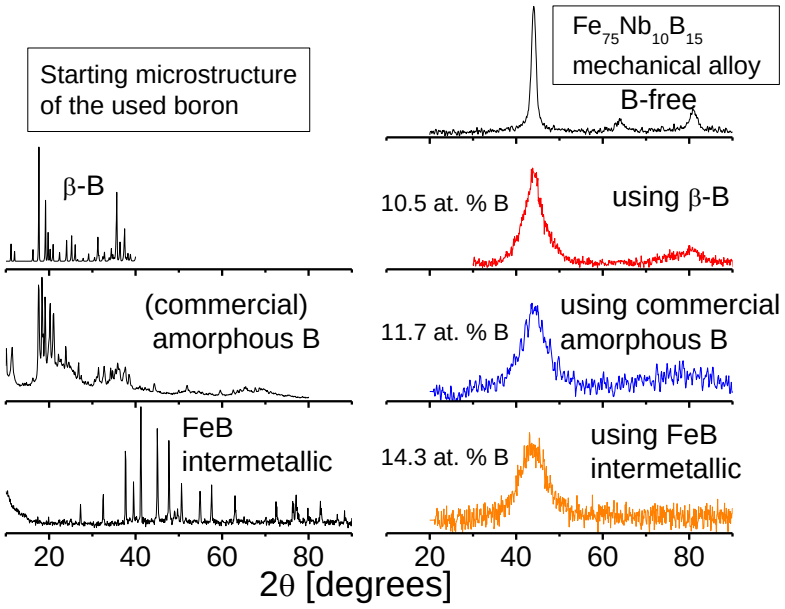

Figure 6. XRD patterns of the starting boron used (left) and the corresponding supersaturated solid solution formed after 40 h of milling at 350 rpm in a Fritsch P4 Pulverisette mill. The crystalline XRD pattern of a B free alloy obtained in the same conditions is also shown for comparison.

The detection of nanometric boron inclusions can be better done using electron microscopy. Preferably, transmission electron microscopy (TEM) where the very thin slice of sample probed, comparable to the size of the inclusions, allows to identify them as hole-like structures due to the very low electron scattering power of boron. However, scanning electron microscopy (SEM) can also be used to identify tiny boron inclusions in transition metal-matrix using the backscattered electrons mode (Z contrast). The inclusions are much better resolved when a flat surface is explored and thus, the use of focus ion beam (FIB) to prepare in situ such surface is very helpful. Figure 7 shows some examples of these boron inclusions as observed in as-milled powder using a conventional SEM, in a surface prepared by FIB, and using a TEM exploring a thin slice prepared by the lift-out procedure in a FIB, which allows us to obtain a constant thickness in the sample.

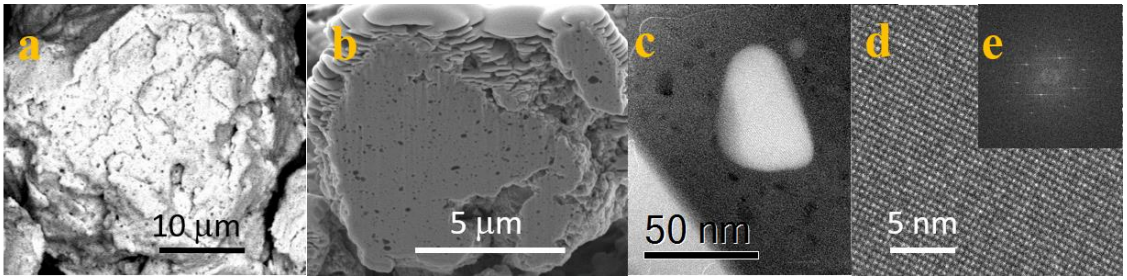

Figure 7. Backscattered SEM images on a $Co_{62}Nb_6Zr_2B_{30}$ mechanically alloyed powder particle (a) as-milled and (b) a polished surface prepared by FIB (Boron particles appear as dark spots in both a and b). TEM images of a $Fe_{75}Nb_{10}B_{15}$ mechanically alloyed powder particle, (c) bright field energy filtered TEM image (boron particle is bright, whereas α-Fe nanocrystals appear darker than the matrix due to diffraction contrast), (d) high resolution TEM image with (e) the corresponding Fourier transform.

4.2 $La(Fe,Si)_{13}$ intermetallic

One of the advantages of mechanical alloying with respect to conventional melting techniques is the capacity of mixing elements with low miscibility. Therefore, it can be used as a first step to obtain a homogeneously mixed alloy that, after suitable annealing, will lead to the formation of an intermetallic phase. This is the case for the fcc $La(Fe,Si)_{13}$ phase. This system, with very interesting magnetocaloric properties [94], requires conventional annealing times of the order of several days. However, this annealing time can be reduced below one hour when the precursor alloy to be annealed is homogenized at the nanoscale, e.g. by rapid quenching methods [106] or by mechanical alloying [60, 61]. Annealing time can be further reduced sintering by SPS [67]. In mechanically alloyed samples, which are the interesting ones in the present study, the formation of a monocrystalline supersaturated solid solution should indicate the formation of this precursor homogeneous alloy. In this study we prepared supersaturated solid solutions with the nominal composition $LaFe_{11.5}Si_{1.5}$ starting from different microstructures: a) pure element powders; b) LaSi intermetallic plus pure Fe and Si; c) LaFeSi intermetallic plus pure Fe and Si; and d) a pulverized $LaFe_{11.5}Si_{1.5}$ arc-melted ingot.

Figure 8 shows the supersaturated solid solution formed from the different starting microstructures. It is evident that using pure La is detrimental for the formation of the supersaturated solid solution which is delayed from 0.5 h for the other systems to 5 h for the mechanically alloyed mixture of pure elements. This is due to the positive enthalpy of mixing of La and Fe [57], which do not form any intermetallic compound in the binary phase diagram.

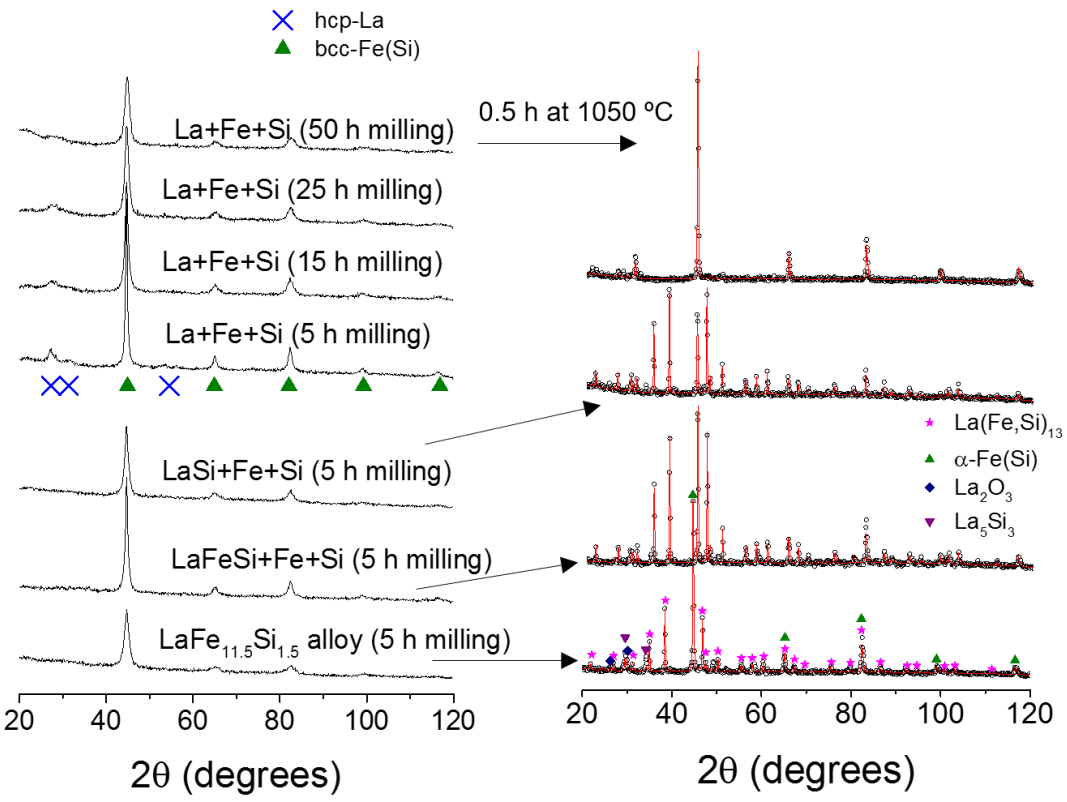

Figure 8. XRD patterns of as-milled powders (left) and annealed powders (right) of $LaFe_{11.5}Si_{1.5}$ composition from different starting microstructures.

Once the supersaturated solid solution is formed, the different systems were annealed at the same conditions (30 min at 1323 K). Figure 8 also shows these XRD patterns. The amount of the desired fcc $La(Fe,Si)_{13}$ phase (obtained from Rietvelf fittings) shows no correlation with the crystal size or microstrains of the supersaturated solid solution (the width of the (110) maximum of α-Fe type phase shows no monotonous trend with the final fraction of fcc phase). However, it seems to be related to the lattice parameter of this metastable phase. Considering a linear increase of the lattice parameter of the bcc supersaturated phase, a_{bcc}, with the La content, under hard spheres approximation, and taking into account the lattice parameters of bcc $Fe_{0.886}Si_{0.114}$ [107] and fcc-La [108], the La content inside the supersaturated solution could be estimated as:

$$x_{La} = \frac{a_{bcc} - a_{\alpha-FeSi}}{\sqrt{\frac{2}{3}}a_{fcc-La} - a_{\alpha-FeSi}} \qquad (8)$$

where $a_{\alpha\text{-}FeSi}$ and $a_{fcc\text{-}La}$ are the lattice parameter of bcc $Fe_{0.886}Si_{0.114}$ and fcc La, respectively. The expansion due to nanosized crystalline phase or other defects are neglected [3]). As a complete incorporation of La inside the supersaturated solid solution would correspond to slightly above

7 at. % of La, results shown in figure 9 point to a poor incorporation of La into the supersaturated bcc phase. However, when La content in the supersaturated solution is above 1 at. %, the amount of La(Fe,Si)$_{13}$ phase obtained after annealing is clearly enhanced.

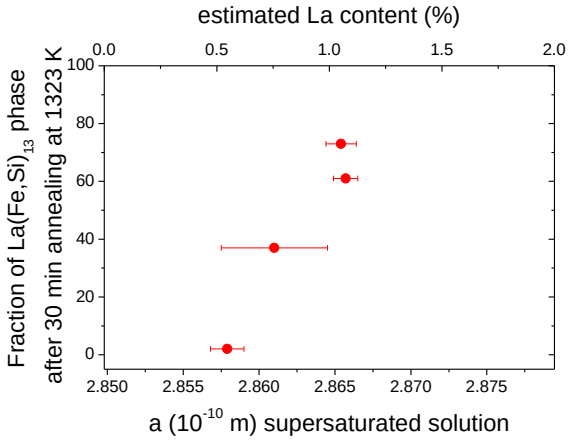

Figure 9. Fraction of $NaZn_{13}$-type phase produced after annealing as a function of the lattice parameter and estimated La content of the supersaturated solution obtained after milling $LaFe_{11.5}Si_{1.5}$ composition from different starting microstructures.

5 Effect of demagnetizing field on MCE characterization

Demagnetizing field, H_D, is a factor to take into account when characterizing magnetic properties of samples from mechanical alloying or milling and, in general, powder samples. This demagnetizing field is produced by the free poles at the edges of the sample but it is only homogeneous for ellipsoidal shapes (where magnetization is homogeneous too). In these cases, the demagnetizing factor N_D can be defined as the ratio between the demagnetizing field and the magnetization and thus the total magnetic field inside the sample, H, should be:

$$H = H_{app} - N_D M \tag{9}$$

where H_{app} is the applied magnetic field and M is the magnetization.

Typical spheroidal powder cannot be aligned to the field to give a negligible N_D and a rough approximation should be to consider N_D=1/3, which is the value corresponding to any direction for a spherical particle. Coey [109] registered an approximation to the demagnetizing factor of a set of particles:

$$N_D^{total} = N_D^{particle} + f\left(N_D^{pack} - N_D^{particle}\right) \tag{10}$$

where N_D^{total}, $N_D^{particle}$, and N_D^{pack} are the demagnetizing factors of the whole sample, the powder particle and the pack, and f is the packing fraction. Therefore, assuming that the pack is a thin plate or needle to minimize N_D^{pack}~0, N_D^{total} would vary between $N_D^{particle}$~1/3 for f=0

and N_D^{pack}~0, for f=1. However, packing fractions close to 1 implies hot pressing techniques and, consequently, thermal treatments that can destroy the metastable phases produced after milling. Sometimes it is not possible to produce a pack with a negligible N_D and Eq.(10) should be used to estimate the value but the value of f is needed. When the pack is also a sphere, N_D^{pack}~1/3 independently of the packing fraction. To obtain the same for non-spherical powder, the pack should have the same aspect ratio as the powder to obtain N_D independent of the packing fraction.

An effective N_D can be estimated from experimental data of the thermal and field dependence of the inverse apparent susceptibility, χ_a^{-1}. This magnitude is related to the actual susceptibility, χ, which is the ratio between the magnetization and the magnetic field, as:

$$\chi^{-1} = \frac{H}{M} = \frac{H_{app} - N_D M}{M} = \chi_a^{-1} - N_D \qquad (11)$$

Therefore, for materials with a high magnetic susceptibility, $\chi >> 1/N_D$ and $N_D \sim 1/\chi_a$ can be approximated to the inverse of the apparent susceptibility. This can occur for soft magnets at low fields. There are two conditions that must be fulfilled by the field and thermal dependence of magnetization to be in this situation: M must be independent of temperature in a certain range below the Curie transition and M must be proportional to the applied magnetic field for low enough values of H. In that case, N_D can be estimated as the inverse of the slope of M vs H. Figure 10 exemplifies this procedure for an irregular piece of Gd, where the left plot shows the evolution of the magnetization versus temperature for low fields. At low temperatures, an almost constant value of M can be found for the lowest fields used. When representing these data as a function of H, it is observed a trend to a linear behavior as temperature and field decreases. This limit can be used to estimate N_D~0.09.

In the case of MCE, neglecting the demagnetizing field slightly affects the magnetic entropy change but strongly affects the field dependence of the MCE close to the transition and thus the critical exponent determination [110, 111].

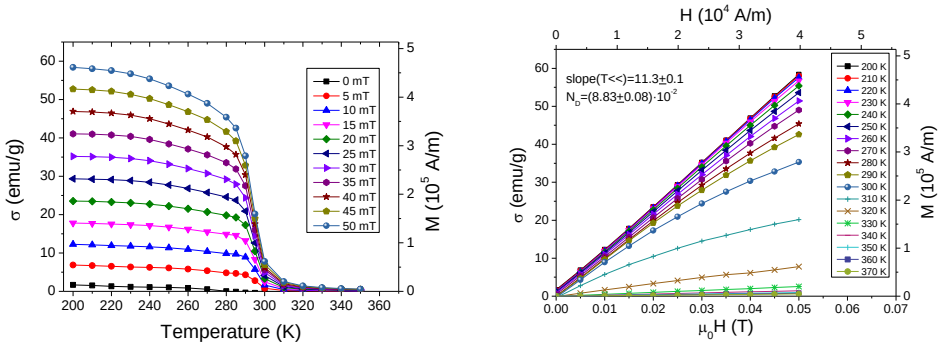

Figure 11. Temperature dependence of the specific magnetization for different field values below 50 mT (left panel). Low field dependence of specific magnetization for different temperatures (right panel).

6 Effect of multiphase character on the MCE

Mechanically alloyed systems or materials subjected to high energy milling are strongly disordered and transitions typically become smeared with respect to those observed in systems obtained by quenching or annealing. On the one hand this fact has the advantage of a wider temperature range in which MCE is noticeable. On the other hand, two wide transitions are not useful as the signal become broad but too weak. In this sense the use of the refrigerant capacity [8] to describe the goodness of a certain material has to be taken with care. The broadening of the transition can be described as a multiphase character of the mechanically alloyed system. This can be found in two different cases: presence of impurity phases (e.g. remnant inclusions) [112] or the existence of a distribution of Curie transitions in highly disordered systems (e.g. in amorphous phases) [111].

The simplest model to afford this problem is to assume non-interacting phases. This implies that the total magnetization is the addition of the magnetization of each phase and thus the magnetic entropy change should be also additive from Maxwell relation:

$$\Delta S^{total} = \mu_0 \int_0^H \left(\frac{d\sigma^{total}}{dT}\Big|_H\right) dH = \mu_0 \sum \int_0^H \left(\frac{d(w_i\sigma_i)}{dT}\Big|_H\right) dH = \sum w_i \Delta S_i \quad (11)$$

where σ^{total} and σ_i are the specific magnetization of the whole system and the *i* phase, respectively, and w_i is the weight fraction of the *i* phase. However, this should not be the case for the adiabatic temperature change:

$$\Delta T_{ad}{}^{total} = -\mu_0 \int_0^H \frac{T}{C_H^{total}} \frac{d\sigma^{total}}{dT}\Big|_H dH = -\mu_0 \sum \int_0^H \frac{T}{C_H^{total}} \frac{d(w_i\sigma_i)}{dT}\Big|_H dH \sim \sum \frac{w_i C_0^i}{C_0^{total}} \Delta T_{ad}{}^i \quad (12)$$

where, as a first approximation, the field dependence of the specific heat c_H, has been neglected and the value at zero field, c_0, has been used. Therefore, impurities with a low Debye temperature are more deleterious concerning the adiabatic temperature change of the sample.

However, the most important effect is observed in the field dependence of the MCE response. The isothermal magnetic entropy change can be written as:

$$\Delta S = aH^n \quad (13)$$

It has been demonstrated that, for single phase systems with a second order phase transition, there are three regions where *n* might be field independent: well below the transition (*n*=1), well above the transition (*n*=2) and at the transition [113]:

$$n = 1 + \frac{\beta - 1}{\beta + \gamma} \quad (14)$$

where β and γ are the critical exponents. However, when the sample is not pure, the experimental exponent departs from these theoretical predictions. This can be understood relating the experimental exponent of the whole system (n_{total}) with those of the different phases.

$$n_{total} = \frac{dln(\Delta S^{total})}{dln(H)} = \sum_i \frac{n_i a_i w_i H^{n_i}}{\Delta S^{total}} \quad (15)$$

We will now simplify the expression (15) assuming two phases: the main phase (index *main*) and the impurity phase (index *imp*). For paramagnetic impurities, measured far above the corresponding T_C, a_{imp}~0 and n_{total} would not be affected. Considering the case of ferromagnetic impurities with T_C far above the measuring temperature, n_{imp}=1 and expression (14) can be written as [114]:

$$n_{total} = \frac{w_{imp} a_{imp} H + w_{main} n_{main} a_{main} H^{n_{main}}}{\Delta S^{total}} = n_{main} + (1 - n_{main}) w_{imp} \frac{a_{imp} H}{\Delta S^{total}} \quad (16)$$

Taking into account Eq. (11), we can write:

$$n_{total} = n_{main} + (1 - n_{main}) w_{imp} \frac{\Delta S^{imp}}{\Delta S^{total}} \quad (17)$$

or

$$\Delta S^{main} = \frac{\Delta S^{total}}{w_{main}} \left(\frac{1 - n_{total}}{1 - n_{main}} \right) \quad (18)$$

From which it should be possible to estimate ΔS^{main} at the transition (value corresponding to a pure phase) from the weight fraction of the main phase (e.g. measured by XRD), the experimental ΔS^{total} and n_{total} values and the expected n_{main} value: i.e. at the transition n_{main} should be dependent on the critical exponents as shown in Eq. (14): e.g. for a mean field system n=2/3). However, it is worth mentioning that, besides the non-interactive phase approach assumed here, the large errors accumulated from the derivation that will affect the quantitative estimation.

From Eq. (17) it is observed that, for values well below T_C, n_{main}=1, there is no effect of the presence of ferromagnetic impurities in the field dependence of MCE response. As temperature increases approaching T_C, n_{main}<1 and thus, the value of the experimental n_{total}>n_{main}. Above the transition n_{main} increases and becomes bigger than 1, thus n_{total}<n_{main}. Therefore, the global effect of the presence of ferromagnetic impurities is to smooth the temperature dependence of n_{total}. It is worth noting that, for ferromagnetic impurities, ΔS^{imp} will monotonously increase as temperature increases. Therefore, taking into account Eq. (17), the effect of the impurities on n_{total} will be bigger as temperature increases. In fact, well above the transition, where n_{main}=2, the trend of n_{total} should exhibit a monotonous decrease. All the features described above are exemplified in figure 11 (data adapted from [112]) for a Fe-Nb-B amorphous alloy with different fractions of remnant α-Fe type crystallites.

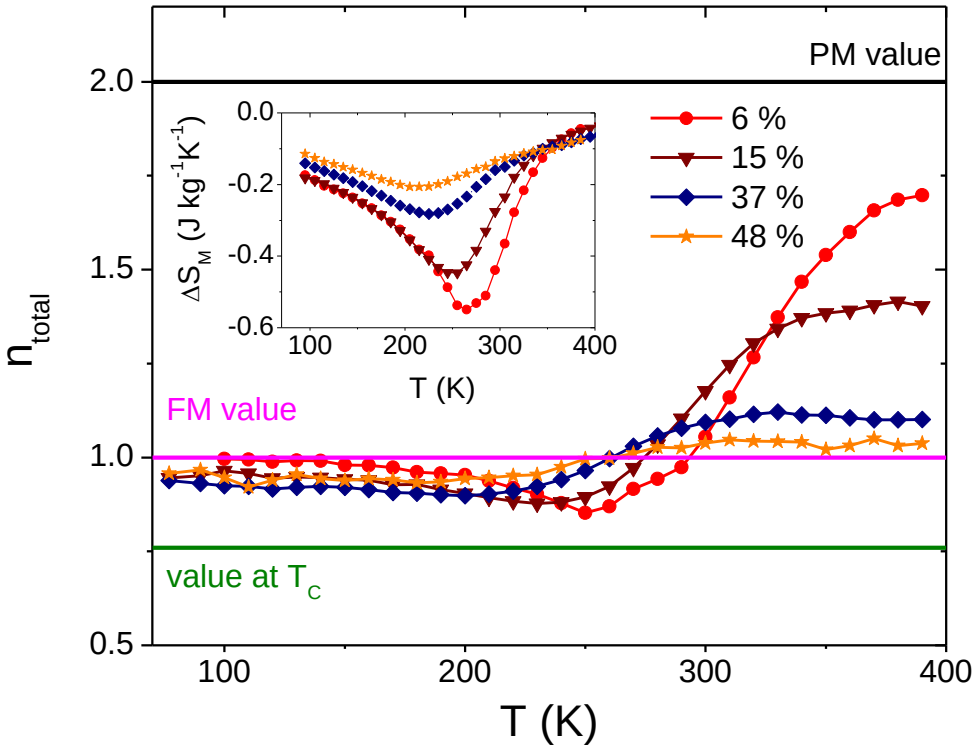

Figure 11. Temperature dependence of the exponent describing the field dependence of the magnetic entropy change for mechanically alloyed amorphous Fe-Nb-B samples with different fractions of α-Fe type nanocrystals. The horizontal lines correspond to the field independent values of n: well below Curie temperature, T_C, (FM value), value at T_C and well above T_C (PM value). Inset: magnetic entropy change for the different samples.

7 Conclusions

In this paper we have reviewed some characteristic aspects of ball milled samples affecting magnetic measurements and, particularly, the magnetocaloric effect.

In order to compare different milling procedures from different labs, simple relations between the geometry and the ratio of the frequencies used are obtained. The existence of optimum milling conditions of these parameters is qualitatively shown.

The state of the art in this research field shows that BM can be used in several ways. Magnetocaloric materials can be directly obtained from mechanical alloying or mechanochemistry methods. Unlike melting methods, BM prevents the loss of volatile elements and leads to compositionally homogeneous precursors in the nanoscale, which reduce the annealing time required to develop the desired intermetallic. Moreover, BM is widely used to easily produce nanocrystalline systems and granular systems and, more recently, mechanically

induced reactions, such as hydriding of $La(FeSi)_{13}$ intermetallic, have been successfully achieved.

Incorporation of boron by mechanical alloying is not trivial and quantification can be difficult. Actual composition of the phases can deviate from the nominal expected ones.

The microstructure of the precursor alloys produced by BM can be optimized to reduce the annealing time needed to develop certain intermetallic phases.

Demagnetizing field is a factor difficult to avoid when dealing with powder. Neglecting it leads to errors in the MCE response and more significantly in its field dependence. Some theoretical and experimental approaches to determine the demagnetizing factor have been described.

Multiphase character of the BM samples, due to remnant impurities or contamination or to distribution of transition temperatures due to induced disordering, particularly affects the field dependence of the MCE response.

Acknowledgements

Spanish Ministry of Science and Innovation and EU FEDER (Projects MAT 2013-45165-P and MAT 2016-77265-R) and the PAI of the Regional Government of Andalucía.

References

[1] Suryanarayana C. Mechanical alloying and milling. Prog Mater Sci. 2001;46:1-184.
[2] Suryanarayana C, Al-Aqeeli N. Mechanically alloyed nanocomposites. Prog Mater Sci. 2013;58:383-502.
[3] Balaz P, Achimovicova M, Balaz M, Billik P, Cherkezova-Zheleva Z, Criado JM, et al. Hallmarks of mechanochemistry: from nanoparticles to technology. Chemical Society reviews. 2013;42:7571-637.
[4] Blazquez JS, Ipus JJ, Lozano-Perez S, Conde A. Metastable Soft Magnetic Materials Produced by Mechanical Alloying: Analysis Using an Equivalent Time Approach. Jom. 2013;65:870-82.
[5] Ipus JJ, Blazquez JS, Franco V, Conde A, Lozano-Perez S. Analysis of the magnetic anisotropy in Fe-Co-Nb-B alloys partially amorphized by mechanical alloying. Physics Express. 2012;2:8.
[6] Ipus JJ, Blázquez JS, Franco V, Conde CF, Conde A. Two milling time regimes in the evolution of magnetic anisotropy of mechanically alloyed soft magnetic powders. Journal of Alloys and Compounds. 2011;509:1407-10.
[7] Hernando A, Vazquez M, Kulik T, Prados C. ANALYSIS OF THE DEPENDENCE OF SPIN-SPIN CORRELATIONS ON THE THERMAL-TREATMENT OF NANOCRYSTALLINE MATERIALS. Physical Review B. 1995;51:3581-6.
[8] Gschneidner KA, Pecharsky VK. Magnetocaloric materials. Annu Rev Mater Sci. 2000;30:387-429.
[9] Franco V, Blázquez JS, Ingale B, Conde A. The Magnetocaloric Effect and Magnetic Refrigeration Near Room Temperature: Materials and Models. Annual Review of Materials Research. 2012;42:305-42.
[10] Blázquez JS, Ipus JJ, Moreno-Ramírez LM, Borrego JM, Lozano-Pérez S, Franco V, et al. Analysis of the Magnetocaloric Effect in Powder Samples Obtained by Ball Milling. Metallurgical and Materials Transactions E. 2015;2:131-8.
[11] Abdellaoui M, Gaffet E. THE PHYSICS OF MECHANICAL ALLOYING IN A PLANETARY BALL MILL - MATHEMATICAL TREATMENT. Acta Metallurgica Et Materialia. 1995;43:1087-98.
[12] Ipus JJ, Blázquez JS, Franco V, Millán M, Conde A, Oleszak D, et al. An equivalent time approach for scaling the mechanical alloying processes. Intermetallics. 2008;16:470-8.
[13] Lebrun P, Froyen L, Delaey L. THE MODELING OF THE MECHANICAL ALLOYING PROCESS IN A PLANETARY BALL MILL - COMPARISON BETWEEN THEORY AND INSITU OBSERVATIONS. Materials Science and Engineering a-Structural Materials Properties Microstructure and Processing. 1993;161:75-82.
[14] Delogu F, Cocco G. Kinetics of structural evolution in immiscible Ag-Cu and Co-Cu systems under mechanical processing conditions. Materials Science and Engineering a-Structural Materials Properties Microstructure and Processing. 2005;402:208-14.
[15] Chevalier B, Bobet JL, Marcos JS, Fernandez JR, Sal JCG. Magnetocaloric properties of amorphous GdNiAl obtained by mechanical grinding. Applied Physics a-Materials Science & Processing. 2005;80:601-6.
[16] Zhang TB, Provenzano V, Chen YG, Shull RD. Magnetic properties of a high energy ball-milled amorphous Gd5Si1.8Ge1.8Sn0.4 alloy. Solid State Communications. 2008;147:107-10.
[17] Shishkin DA, Baranov NV, Gubkin AF, Volegov AS, Gerasimov EG, Terentev PB, et al. Impact of amorphization on the magnetic state and magnetocaloric properties of Gd3Ni. Applied Physics a-Materials Science & Processing. 2014;116:1403-7.
[18] Ipus JJ, Blázquez JS, Franco V, Conde A. Mechanical alloying of Fe100−x−yNbxBy (x=5, 10; y=10, 15): From pure powder mixture to amorphous phase. Intermetallics. 2008;16:1073-82.
[19] Ipus JJ, Blazquez JS, Franco V, Conde A, Kiss LF. Magnetocaloric response of Fe(75)Nb(10)B(15) powders partially amorphized by ball milling. Journal of Applied Physics. 2009;105.

[20] Ipus JJ, Blazquez JS, Franco V, Conde A. Influence of Co addition on the magnetic properties and magnetocaloric effect of Nanoperm (Fe(1-x)Co(x))(75)Nb(10)B(15) type alloys prepared by mechanical alloying. Journal of Alloys and Compounds. 2010;496:7-12.
[21] Moreno LM, Blázquez JS, Ipus JJ, Borrego JM, Franco V, Conde A. Magnetocaloric effect of Co62Nb6Zr2B30 amorphous alloys obtained by mechanical alloying or rapid quenching. Journal of Applied Physics. 2014;115:17A302.
[22] Ipus JJ, Ucar H, McHenry ME. Near Room Temperature Magnetocaloric Response of an (FeNi)ZrB Alloy. IEEE Trans Magn. 2011;47:2494-7.
[23] Ucar H, Craven M, Laughlin DE, McHenry ME. Effect of Mo Addition on Structure and Magnetocaloric Effect in gamma-FeNi Nanocrystals. Journal of Electronic Materials. 2014;43:137-41.
[24] Chaudhary V, Repaka DVM, Chaturvedi A, Sridhar I, Ramanujan RV. Magnetocaloric properties and critical behavior of high relative cooling power FeNiB nanoparticles. Journal of Applied Physics. 2014;116.
[25] Chaudhary V, Ramanujan RV. Magnetic and structural properties of high relative cooling power (Fe70Ni30)(92)Mn-8 magnetocaloric nanoparticles. Journal of Physics D-Applied Physics. 2015;48.
[26] Varzaneh AG, Kameli P, Karimzadeh F, Aslibeiki B, Varvaro G, Salamati H. Magnetocaloric effect in Ni47Mn40Sn13 alloy prepared by mechanical alloying. Journal of Alloys and Compounds. 2014;598:6-10.
[27] Gomes AM, das Virgens MG, Continentino MA, Checon JCC, Lopez A, Azevedo IS. Behavior of the inverse magnetocaloric effect in RuSr(2)Eu(1.5)Ce(0.5)Cu(2)O(10-delta). Journal of Magnetism and Magnetic Materials. 2008;320:E513-E5.
[28] Anwar MS, Ahmed F, Koo BH. Structural distortion effect on the magnetization and magnetocaloric effect in Pr modified La0.65Sr0.35MnO3 manganite. Journal of Alloys and Compounds. 2014;617:893-8.
[29] Zouari S, Ellouze M, Nasri A, Cherif W, Hlil EK, Elhalouani F. Morphology, Structural, Magnetic, and Magnetocaloric Properties of Pr0.7Ca0.3MnO3 Nanopowder Prepared by Mechanical Ball Milling Method. Journal of Superconductivity and Novel Magnetism. 2014;27:555-63.
[30] Rayaprol S, Kaushik SD. Magnetic and magnetocaloric properties of FeMnO3. Ceramics International. 2015;41:9567-71.
[31] Messaoui I, Riahi K, Cheikhrouhou-Koubaa W, Koubaa M, Cheikhrouhou A, Hlil EK. Phenomenological model of the magnetocaloric effect on Nd0.7Ca0.15Sr0.15MnO3 compound prepared by ball milling method. Ceramics International. 2016;42:6825-32.
[32] Schouwink P, Didelot E, Lee Y-S, Mazet T, Cerny R. Structural and magnetocaloric properties of novel gadolinium borohydrides. Journal of Alloys and Compounds. 2016;664:378-84.
[33] Ipus JJ, Borrego JM, Blazquez JS, Stoica M, Franco V, Conde A. Influence of hot compaction on microstructure and magnetic properties of mechanically alloyed Fe(Co)-based amorphous compositions. Journal of Alloys and Compounds. 2015;653:546-51.
[34] Zhong W, Liu W, Wu XL, Tang NJ, Chen W, Au CT, et al. Magnetocaloric effect in the ordered double perovskite Sr2FeMo1-xWxO6. Solid State Communications. 2004;132:157-62.
[35] Zhang P, Yang H, Zhang S, Ge H, Hua S. Magnetic and magnetocaloric properties of perovskite La0.7Sr0.3Mn1-xCoxO3. Physica B-Condensed Matter. 2013;410:1-4.
[36] Zhong W, Wu XL, Tang NJ, Liu W, Chen W, Au CT, et al. Magnetocaloric effect in ordered double-perovskite Ba2FeMoO6 synthesized using wet chemistry. Eur Phys J B. 2004;41:213-7.
[37] Gass J, Srikanth H, Kislov N, Srinivasan SS, Emirov Y. Magnetization and magnetocaloric effect in ball-milled zinc ferrite powder. Journal of Applied Physics. 2008;103:07B309.
[38] Yan A, Muller KH, Schultz L, Gutfleisch O. Magnetic entropy change in melt-spun MnFePGe (invited). Journal of Applied Physics. 2006;99.

[39] Czaja P, Przewoznik J, Fitta M, Balanda M, Chrobak A, Kania B, et al. Effect of ball milling and thermal treatment on exchange bias and magnetocaloric properties of Ni48Mn39.5Sn10.5Al2 ribbons. Journal of Magnetism and Magnetic Materials. 2016;401:223-30.
[40] Songlin, Dagula, Tegus O, Bruck E, de Boer FR, Buschow KHJ. Magnetic and magnetocaloric properties of Mn5Ge3-xSbx. Journal of Alloys and Compounds. 2002;337:269-71.
[41] Bruck E, Tegus O, Zhang L, Li XW, de Boer FR, Buschow KHJ. Magnetic refrigeration near room temperature with Fe2P-based compounds. Journal of Alloys and Compounds. 2004;383:32-6.
[42] Bruck E, Ilyn M, Tishin AM, Tegus O. Magnetocaloric effects in MnFeP1-xAsx-based compounds. Journal of Magnetism and Magnetic Materials. 2005;290:8-13.
[43] Dagula W, Tegus O, Fuquan B, Zhang L, Si PZ, Zhang M, et al. Magnetic-entropy change in Mn1.1Fe0.9P1-xGex compounds. IEEE Trans Magn. 2005;41:2778-80.
[44] Tegus O, Fuquan B, Dagula W, Zhang L, Bruck E, Si PZ, et al. Magnetic-entropy change in Mn1.1Fe0.9P0.7As0.3-xGex. Journal of Alloys and Compounds. 2005;396:6-9.
[45] Dagula W, Tegus O, Li XW, Song L, Bruck E, Thanh DTC, et al. Magnetic properties and magnetic-entropy change of MnFeP0.5As0.5-xSix(x=0-0.3) compounds. Journal of Applied Physics. 2006;99:08Q105.
[46] Lozano JA, Kostow MP, Bruck E, de Lima JC, Prata AT, Wendhausen PAP. Porous manganese-based magnetocaloric material for magnetic refrigeration at room temperature. Journal of Magnetism and Magnetic Materials. 2008;320:E189-E92.
[47] Yue M, Li ZQ, Xu H, Huang QZ, Liu XB, Liu DM, et al. Effect of annealing on the structure and magnetic properties of Mn1.1Fe0.9P0.8Ge0.2 compound. Journal of Applied Physics. 2010;107.
[48] Liu DM, Yue M, Zhang JX, McQueen TM, Lynn JW, Wang XL, et al. Origin and tuning of the magnetocaloric effect in the magnetic refrigerant Mn1.1Fe0.9(P0.8Ge0.2). Physical Review B. 2009;79:014435.
[49] Zhang L, Bruck E, Tegus O, Buschow KHJ, de Boer FR. The crystallographic phases and magnetic properties of Fe2MnSi1-xGex. Physica B-Condensed Matter. 2003;328:295-301.
[50] Bruck E, Tegus O, Thanh DTC, Trung NT, Buschow KHJ. A review on Mn based materials for magnetic refrigeration: Structure and properties. International Journal of Refrigeration-Revue Internationale Du Froid. 2008;31:763-70.
[51] Yibole H, Guillou F, Caron L, Jimenez E, de Groot FMF, Roy P, et al. Moment evolution across the ferromagnetic phase transition of giant magnetocaloric (Mn, Fe)(2)(P, Si, B) compounds. Physical Review B. 2015;91.
[52] Sun NK, Cui WB, Li D, Geng DY, Yang F, Zhang ZD. Giant room-temperature magnetocaloric effect in Mn(1-x)Cr(x)As. Applied Physics Letters. 2008;92.
[53] Cui WB, Liu W, Zhang Q, Li B, Liu XH, Yang F, et al. Carbon-doping effects on the metamagnetic transition and magnetocaloric effect in MnAsCx. Journal of Magnetism and Magnetic Materials. 2010;322:2223-6.
[54] Cui WB, Lv XK, Yang F, Yu Y, Skomski R, Zhao XG, et al. Interstitial-nitrogen effect on phase transition and magnetocaloric effect in Mn(As,Si) (invited). Journal of Applied Physics. 2010;107:09A938.
[55] Sun NK, Li D, Xu SN, Wang ZH, Zhang ZD. Room-temperature Magnetocaloric Effect in (Co(0.35)Mn(0.65))(2)P Compound. Journal of Materials Science & Technology. 2011;27:382-4.
[56] Ma L, Guillou F, Yibole H, Miao XF, Lefering AJE, Rao GH, et al. Structural, magnetic and magnetocaloric properties of (Mn, Co)(2)(Si, P) compounds. Journal of Alloys and Compounds. 2015;625:95-100.
[57] de Boer FR, Boom R, Mattens WCM, Miedema AR, Niessen AK. Cohesion in Metals. Amsterdam: Elsevier Science Pub. B.V.; 1988.

[58] Passamani EC, Takeuchi AY, Alves AL, Demuner AS, Favre-Nicolin E, Larica C, et al. Magnetocaloric properties of (La,RE)Fe11.4Si1.6 compounds (RE=Y,Gd). Journal of Applied Physics. 2007;102:093906.
[59] Cui WB, Liu W, Liu XH, Guo S, Han Z, Zhao XG, et al. Beneficial effect of minor Al substitution on the magnetocaloric effect of Mn1-xAlxAs. Mater Lett. 2009;63:595-7.
[60] Phejar M, Paul-Boncour V, Bessais L. Structural and magnetic properties of magnetocaloric LaFe(13-x)Si(x) compounds synthesized by high energy ball-milling. Intermetallics. 2010;18:2301-7.
[61] Phejar M, Paul-Boncour V, Bessais L. Investigation on structural and magnetocaloric properties of LaFe13-xSix(H,C)(y) compounds. Journal of Solid State Chemistry. 2016;233:95-102.
[62] Guetari R, Bez R, Cizmas CB, Mliki N, Bessais L. Magnetic properties and magneto-caloric effect in pseudo-binary intermetallic (Pr,Dy)(2)Fe-17. Journal of Alloys and Compounds. 2013;579:156-9.
[63] Bulatova R, Bahl C, Andersen K, Kuhn LT, Pryds N. Functionally Graded Ceramics Fabricated with Side-by-Side Tape Casting for Use in Magnetic Refrigeration. International Journal of Applied Ceramic Technology. 2015;12:891-8.
[64] Lanzarini J, Barriere T, Sahli M, Gelin JC, Dubrez A, Mayer C, et al. Thermoplastic filled with magnetocaloric powder. Materials & Design. 2015;87:1022-9.
[65] Liu DM, Zhang H, Wang SB, Xiao WQ, Zhang ZL, Tian N, et al. The effect of Al doping on the crystal structure and magnetocaloric behavior of Mn1.2Fe0.8P1-xGex compounds. Journal of Alloys and Compounds. 2015;633:120-6.
[66] Kaeswurm B, Friemert K, Guersoy M, Skokov KP, Gutfleisch O. Direct measurement of the magnetocaloric effect in cementite. Journal of Magnetism and Magnetic Materials. 2016;410:105-8.
[67] Patissier A, Paul-Boncour V. Fast synthesis of LaFe13-xSix magnetocaloric compounds by reactive Spark Plasma Sintering. Journal of Alloys and Compounds. 2015;645:143-50.
[68] Bartok A, Kustov M, Cohen LF, Pasko A, Zehani K, Bessais L, et al. Study of the first paramagnetic to ferromagnetic transition in as prepared samples of Mn-Fe-P-Si magnetocaloric compounds prepared by different synthesis routes. Journal of Magnetism and Magnetic Materials. 2016;400:333-8.
[69] Kupseh A, Levin AA, Meyer DC. Structural phase transition in Tb-5(Si0.6Ge0.4)(4) at low temperature. Crystal Research and Technology. 2005;40:42-51.
[70] Gao Q, Yu BF, Wang CF, Zhang B, Yang DX, Zhang Y. Experimental investigation on refrigeration performance of a reciprocating active magnetic regenerator of room temperature magnetic refrigeration. International Journal of Refrigeration-Revue Internationale Du Froid. 2006;29:1274-85.
[71] Rajkumar DM, Raja MM, Gopalan R, Chandrasekaran V. Magnetocaloric effect in high-energy ball-milled Gd5Si2Ge2 and Gd5Si2Ge2/Fe nanopowders. Journal of Magnetism and Magnetic Materials. 2008;320:1479-84.
[72] Chrobak A, Bajorek A, Chelkowska G, Haneczok G, Kwiecien M. Magnetic properties and magnetocaloric effect of Gd(Ni(1-x)Fe(x))(3) crystalline compound and powder. Physica Status Solidi a-Applications and Materials Science. 2009;206:731-7.
[73] Pires AL, Belo JH, Turcaud J, Oliveira GNP, Araujo JP, Berenov A, et al. Influence of short time milling in R-5(Si,Ge)(4), R = Gd and Tb, magnetocaloric materials. Materials & Design. 2015;85:32-8.
[74] Ipus JJ, Blazquez JS, Franco V, Stoica M, Conde A. Milling effects on magnetic properties of melt spun Fe-Nb-B alloy. Journal of Applied Physics. 2014;115.
[75] Shao Y, Zhang J, Lai JKL, Shek CH. Magnetic entropy in nanocomposite binary gadolinium alloys. Journal of Applied Physics. 1996;80:76.

[76] Llamazares JLS, Perez MJ, Alvarez P, Santos JD, Sanchez ML, Hernando B, et al. The effect of ball milling in the microstructure and magnetic properties of Pr2Fe17 compound. Journal of Alloys and Compounds. 2009;483:682-5.
[77] Alvarez P, Gorria P, Franco V, Marcos JS, Perez MJ, Llamazares JLS, et al. Nanocrystalline Nd2Fe17 synthesized by high-energy ball milling: crystal structure, microstructure and magnetic properties. Journal of Physics-Condensed Matter. 2010;22:216005.
[78] Zhang XY, Chen YJ, Lu LY, Li ZY. A potential oxide for magnetic refrigeration application: CrO2 particles. Journal of Physics-Condensed Matter. 2006;18:L559-L66.
[79] Das SD, Mohapatra N, Iyer KK, Bapat RD, Sampathkumaran EV. Magnetic behavior of nanocrystalline ErCo(2). Journal of Physics-Condensed Matter. 2009;21:296004.
[80] Phan MH, Morales MB, Chinnasamy CN, Latha B, Harris VG, Srikanth H. Magnetocaloric effect in bulk and nanostructured Gd(3)Fe(5)O(12) materials. Journal of Physics D-Applied Physics. 2009;42:115007.
[81] Alves AL, Passamani EC, Nascimento VP, Takeuchi AY, Larica C. Influence of grain refinement and induced crystal defects on the magnetic properties of Ni50Mn36Sn14 Heusler alloy. Journal of Physics D-Applied Physics. 2010;43.
[82] Das R, Perumal A, Srinivasan A. Effect of particle size on the magneto-caloric properties of Ni51Mn34In14Si1 alloy. Journal of Alloys and Compounds. 2013;572:192-8.
[83] do Couto GG, Svitlyk V, Jafelicci M, Mozharivskyj Y. Bulk and high-energy ball-milled Gd(5)Si(2)Ge(2): Comparative study of magnetic and magnetocaloric properties. Solid State Sciences. 2011;13:209-15.
[84] Couillaud S, Chevalier B, Paul-Boncour V, Bobet JL. On the magnetic properties of pseudo-Laves phases RE1-yYyNi4-xAlxMg with RE = La, Ce and Gd prepared by both melting and ball milling. Journal of Alloys and Compounds. 2012;525:166-71.
[85] Maji B, Suresh KG, Chen X, Ramanujan RV. Magnetic and magnetocaloric properties of ball milled Nd5Ge3. Journal of Applied Physics. 2012;111:073905.
[86] The-Long P, Thanh TD, Zhang P, Yang DS, Yu SC. The magnetic phase transition and magnetocaloric effect in Sm0.58Sr0.42MnO3 nanoparticles. Solid State Communications. 2013;166:32-7.
[87] Tran Dang T, Dinh Chi L, Hoang Thanh V, Thi Anh H, Tien Van M, Le Viet B, et al. Magnetocaloric Effect in La0.7Ca0.25Ba0.05MnO3 Nanocrystals Exhibiting the Crossover of First- and Second-Order Magnetic Phase Transformation. Materials Transactions. 2015;56:1316-9.
[88] Biswas A, Chandra S, Stefanoski S, Blazquez JS, Ipus JJ, Conde A, et al. Enhanced cryogenic magnetocaloric effect in Eu8Ga16Ge30 clathrate nanocrystals. Journal of Applied Physics. 2015;117.
[89] Kaya M, Rezaeivala M, Yuzuak E, Akturk S, Dincer I, Elerman Y. Effects of size reduction on the magnetic and magnetocaloric properties of NdMn2Ge2 nanoparticles prepared by high-energy ball milling. Physica Status Solidi B-Basic Solid State Physics. 2015;252:192-7.
[90] de Santanna YVB, de Melo MAC, Santos IA, Coelho AA, Gama S, Cotica LF. Structural, microstructural and magnetocaloric investigations in high-energy ball milled Ni2.18Mn0.82Ga powders. Solid State Communications. 2008;148:289-92.
[91] Paticopoulos SC, Caballero-Flores R, Franco V, Blázquez JS, Conde A, Knipling KE, et al. Enhancement of the magnetocaloric effect in composites: Experimental validation. Solid State Communications. 2012;152:1590-4.
[92] Jones NJ, Ucar H, Ipus JJ, McHenry ME, Laughlin DE. The effect of distributed exchange parameters on magnetocaloric refrigeration capacity in amorphous and nanocomposite materials. Journal of Applied Physics. 2012;111.
[93] Nersessian N, Or SW, Carman GP, McCall SK, Choe W, Radousky HB, et al. Gd5Si2Ge2 composite for magnetostrictive actuator applications. Applied Physics Letters. 2004;84:4801-3.

[94] Fujieda S, Fujita A, Fukamichi K. Large magnetocaloric effects in NaZn13-type La(FexSi1-x)(13) compounds and their hydrides composed of icosahedral clusters. Science and Technology of Advanced Materials. 2003;4.
[95] Mandal K, Gutfleisch O, Yan A, Handstein A, Muller KH. Effect of reactive milling in hydrogen on the magnetic and magnetocaloric properties of LaFe11.57Si1.43. Journal of Magnetism and Magnetic Materials. 2005;290:673-5.
[96] Mandal K, Pal D, Gutfleisch O, Kerschl P, Muller KH. Magnetocaloric effect in reactively-milled LaFe11.57Si1.43Hy intermetallic compounds. Journal of Applied Physics. 2007;102:053906.
[97] Lyubina J, Gutfleisch O, Kuz'min MD, Richter M. La(Fe,Si)(13)-based magnetic refrigerants obtained by novel processing routes. Journal of Magnetism and Magnetic Materials. 2008;320:2252-8.
[98] Sun NK, Xu SN, Li D, Zhang ZD. Magnetocaloric effect and size-effect related thermal hysteresis reduction in MnAs1-xPx compounds. Physica Status Solidi a-Applications and Materials Science. 2011;208:1950-2.
[99] Yoshizawa Y, Oguma S, Yamauchi K. NEW FE-BASED SOFT MAGNETIC-ALLOYS COMPOSED OF ULTRAFINE GRAIN-STRUCTURE. Journal of Applied Physics. 1988;64:6044-6.
[100] Kirchner A, Grunberger W, Gutfleisch O, Neu V, Muller KH, Schultz L. A comparison of the magnetic properties and deformation behaviour of Nd-Fe-B magnets made from melt-spun, mechanically alloyed and HDDR powders. Journal of Physics D-Applied Physics. 1998;31:1660-6.
[101] Moreno LM, Blázquez JS, Ipus JJ, Conde A. Amorphization and evolution of magnetic properties during mechanical alloying of Co62Nb6Zr2B30: Dependence on starting boron microstructure. Journal of Alloys and Compounds. 2014;585:485-90.
[102] Ipus JJ, Blázquez JS, Lozano-Perez S, Conde A. Microstructural evolution characterization of Fe–Nb–B ternary systems processed by ball milling. Philosophical Magazine. 2009;89:1415-23.
[103] Doyle PA, Turner PS. Relativistic Hartree-Fock X-ray and Electron Scattering Factors. Acta Crystallographica A. 1968;24:390-7.
[104] Ipus JJ, Blázquez JS, Conde CF, Borrego JM, Franco V, Lozano-Pérez S, et al. Relationship between mechanical amorphization and boron integration during processing of FeNbB alloys. Intermetallics. 2014;49:98-105.
[105] Wijn HPJ. Landolt-Börnstein: Magnetische Eigenschaften von Metallen. Berlin: Springer; 1991.
[106] Liu XB, Liu XD, Altounian Z, Tu GH. Phase formation and structure in rapidly quenched La(Fe0.88Co0.12)(13-x)Si-x alloys. Journal of Alloys and Compounds. 2005;397:120-5.
[107] Tarasov LP. Ferromagnetic Anisotropy of Iron and Iron-Rich Silicon Alloys. Physical Review. 1939;56:1231-40.
[108] Hill HH, Ellinger FH. The effective size of americium dissolved in lanthanum. Journal of Less-Common Metals. 1971;23:92-4.
[109] Coey JMD. Magnetism and Magnetic Materials. New York: Cambridge University Press 2010.
[110] Romero-Muñiz C, Ipus JJ, Blázquez JS, Franco V, Conde A. Influence of the demagnetizing factor on the magnetocaloric effect: Critical scaling and numerical simulations. Applied Physics Letters. 2014;104:252405.
[111] Moreno-Ramírez LM, Ipus JJ, Franco V, Blázquez JS, Conde A. Analysis of magnetocaloric effect of ball milled amorphous alloys: Demagnetizing factor and Curie temperature distribution. Journal of Alloys and Compounds. 2015;622:606-9.
[112] Ipus JJ, Moreno-Ramirez LM, Blazquez JS, Franco V, Conde A. A procedure to extract the magnetocaloric parameters of the single phases from experimental data of a multiphase system. Applied Physics Letters. 2014;105.

[113] Franco V, Blázquez JS, Conde A. Field dependence of the magnetocaloric effect in materials with a second order phase transition: A master curve for the magnetic entropy change. Applied Physics Letters. 2006;89:222512.
[114] Blázquez JS, Moreno-Ramírez LM, Ipus JJ, Kiss LF, Kaptás D, Kemény T, et al. Effect of α-Fe impurities on the field dependence of magnetocaloric response in LaFe11.5Si1.5. Journal of Alloys and Compounds. 2015;646:101-5.